Hindawi Publishing Corporation
Smart Materials Research
Volume 2013, Article ID 271546, 12 pages
http://dx.doi.org/10.1155/2013/271546

Research Article

Self-Healing of Ionomeric Polymers with Carbon Fibers from Medium-Velocity Impact and Resistive Heating

Vishnu Baba Sundaresan,[1] Andrew Morgan,[1] and Matt Castellucci[2]

[1] *Mechanical Engineering Department, Virginia Commonwealth University, Richmond, VA 23284, USA*
[2] *Center for Intelligent Materials Systems and Structures, Virginia Tech, Blacksburg, VA 24061, USA*

Correspondence should be addressed to Vishnu Baba Sundaresan; sundaresan.19@osu.edu

Received 2 October 2012; Revised 24 March 2013; Accepted 27 March 2013

Academic Editor: Yanjun Zheng

Self-healing materials science has seen significant advances in the last decade. Recent efforts have demonstrated healing in polymeric materials through chemical reaction, thermal treatment, and ultraviolet irradiation. The existing technology for healing polymeric materials through the aforementioned mechanisms produces an irreversible change in the material and makes it unsuitable for subsequent healing cycles. To overcome these disadvantages, we demonstrate a new composite self-healing material made from an ionomer (Surlyn) and carbon fiber that can sustain damage from medium-velocity impact and heal from the energy of the impact. Furthermore, the carbon fiber embedded in the polymer matrix results in resistive heating of the polymer matrix locally, melts the ionomer matrix around the damage, and heals the material at the damaged location. This paper presents methods to melt-process Surlyn with carbon fiber and demonstrates healing in the material through medium-velocity impact tests, resistive heating, and imaging through electron and optical microscopy. A new metric for quantifying self-healing in the sample, called width-heal ratio, is developed, and we report that the Surlyn-carbon fiber-based material under an optimal rate of heating and at the correct temperature has a width-heal ratio of >0.9, thereby demonstrating complete recovery from the damage.

1. Introduction

Damage detection and self-healing are unique properties of biological materials and systems. In such systems, a damage event triggers internal processes that generate the healing response and extend the life of the material. This unique property of biological materials has served as the inspiration for self-healing materials in engineering. In the most common self-healing concepts developed to date, damage events are directly or electronically coupled to the release of the healing agents to heal the damage in the material.

The most commonly used healing agents such as chemical binders, heat, and light alter the chemical composition and microstructure of the material to heal the damage and restore strength at the damage site. The capsule-based method developed by White and coworkers [1–4] uses a chemical binder that is released into the matrix of the composite material in the event of a damage. The binder combines with the matrix or hardening agent present in adjacent microcapsule to heal the damage. A variation of the microcapsule-based technique uses vascular networks filled with healing agents to heal structural damage [5–12]. In another variation of this method, hollow glass fibers filled with healing agents are built into the material that releases the binding agents during a damage event. These hollow glass fibers in few designs are woven into the matrix structure [13–17] and heal damage even in a thin cross-sections. These chemical binder-based methods change the material composition at the damage site during healing and hence can be used to heal a damaged site in this material only once. Besides these chemical binders-based methods, thermal methods to heal a damage have been investigated for structural polymers (mendable polymers or "mendomers") [18–20]. The heat required for healing in mendomers is provided by a processes extrinsic to the material and at a time chosen by the damage detection method. In another thermal method, Kalista [21] uses an ionomeric polymer (Surlyn) to demonstrate autonomous self-healing. In this material, heat generated during the damage event such as ballistic impact is harnessed to melt the polymer at the damage location to heal the damage [22–25]. While the Surlyn ionomer used

by Kalista [21], Kalista and Ward [22], and Varley and Van der Zwaag [23, 24] demonstrates an interesting concept, it does not apply to damage occurring in a material during regular wear and tear. To advance the use of Surlyn in self-healing, Owen [26] developed a novel approach to mitigate this deficiency with Surlyn by dispersing magnetic particles in Surlyn. This method, while taking a step in the right direction, requires a large induction coil to heal the damage in the sample. In addition to these methods, self-healing methods presented in the review paper by Wu et al. [27], self-healing sensor skin [28], bioinspired methods developed by Trask et al. [5, 14], and recent work by White group [29] demonstrate novel techniques for healing structural damages. Alongside the work reported in this paper, there has been a renewed interest in thermoplastic polymers that use reversible ionic aggregation to function as self-healing materials [12, 30, 31].

The current state-of-the-art in self-healing, with the exception of some thermal and photochemical methods, requires chemical modification to the structure and cannot be healed at a damage site after one damage event. While photochemical self-healing has proved to be able to induce repeated healing of damages at the same damage site, it lacks the structural capabilities of a desired self-healing composite. It is evident that a chemical binder, once consumed, cannot be regenerated after the healing process is complete. In addition, the chemical binder-based methods that use microcapsules and vascular networks for healing a damage require a minimum volume of the binder filled in the hollow cavity to heal the material. The microcapsules or vascular networks are practically obtrusive for use in thin polymer films such as wire-insulation material in aerospace applications. The work presented in this paper is motivated by the need to develop a self-healing technique for thin membranes that can be repeatedly healed by the application of heat. It is anticipated that this composite material discussed in this paper will be useful as *one of the layers of a* wire-insulation composite, inflatable membranes, and aerodynamic surfaces of micro-air-vehicles and in various aerospace applications.

2. Surlyn-Carbon Fiber Self-Healing Composite

The self-healing material presented in this paper is a composite material prepared by embedding carbon fibers in Surlyn 8940 (referred to as "Surlyn" from this point forward). Surlyn is an ethylene/methacrylic acid (E/MAA) copolymer in which the MAA groups are partially neutralized with sodium ions. This sodium ionomer is chosen as the matrix of the self-healing composite for its low melt temperature of 95°C and previously demonstrated healing capabilities. Carbon fibers are selected as a heating element due to its low electrical resistance, resistive heating property, and reinforcement properties. Other properties, such as low density and high strength, make this an attractive option over other heating elements. The carbon fiber fabric used in this work is obtained from Aerospace Composite Products. There are many possible arrangements of carbon fiber bundles in Surlyn. Typically, carbon fiber structural composite materials are manufactured using layers of a woven fabric containing a few thousand reinforcing fibers stacked in different angular orientations. Carbon fiber bundles in the self-healing composite demonstrated in this paper are arranged in a unidirectional pattern between two layers of Surlyn sheets (200 μm thick) and melt-pressed into a composite. For testing and characterization, two configurations of carbon fiber in Surlyn is fabricated for this work. In the first configuration, the carbon fibers are uniformly distributed in the matrix. In the second configuration, bundles of carbon fibers are distributed throughout the sample with finite spacing between adjacent bundles. Each bundle containing 1000 carbon fiber threads is used as a singular unit. The carbon fibers distributed in the composite are exposed at the two ends (or) internally connected to copper wires of the pressed sheet for electrical access. Examples of fabricated samples are shown in Figure 1(a). In order to achieve uniform resistive heating, the composite in Figure 1 is proposed to be used as individually addressable coupons that will be electrically heated by the healing circuit for healing. In addition, the electrical resistance of the carbon fiber bundles in the coupons is kept to a minimum to achieve faster heating and hence a quick healing response. The electrical resistance of the bundles measuring 20 mm long is kept within 5–10 Ω. These self-healing coupons are targeted to be used as a healing layer and applied as shown in Figure 1(b).

2.1. Fabrication of the Self-Healing Composite. Surlyn is obtained in the form of 1 mm pellets from DuPont. Films of different thicknesses (150 μm, 200 μm, and 400 μm) are produced by compressing Surlyn pellets in a melt press. Steel shims are used between the top and bottom plates in the melt press to maintain uniform thickness. The melt press is operated at 160°C and 3.5 MPa for 30 s to produce a clear Surlyn film. Increasing press time, temperature, or pressure does not significantly alter the film thickness or improve clarity of the films. Polyimide release films are used to prevent the sheets from sticking onto the hot plate. During melt pressing, additional care is taken to avoid trapped air in the sheets. Films with trapped air are stacked together and repressed into sheets to eliminate air pockets. Surlyn films thus obtained are cut to size and used for subsequent processing. A three-layer stack of Surlyn/carbon fiber/Surlyn is prepared and pressed into the self-healing composite. The stack is heated up to 160°C on a VWR hot plate with a 500 g dead weight and held for 5 m. The resulting composite shown in Figure 1 is used to demonstrate healing and characterize the healing process. A step-by-step illustration of the fabrication method is shown in Figure 2.

2.2. Medium-Velocity Impact Testing. The experimental setup required for characterizing the healing in the polymer coupon during a projectile impact and penetration is shown in Figure 3. The setup comprises of a Lexan containment chamber with a partition at the center of the chamber. The partition contains a sample holder that will accommodate the sample and firmly secure it during impact. A Crossman 2100 air rifle is used for delivering a projectile traveling at

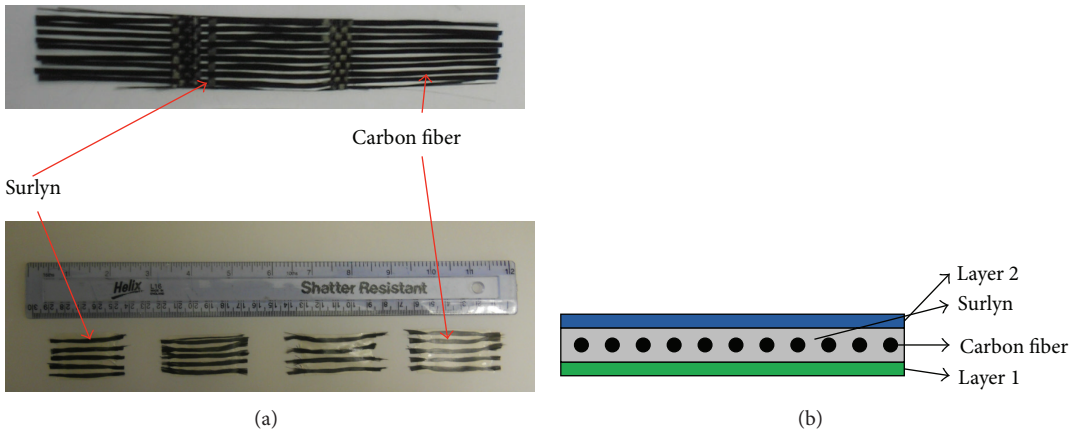

FIGURE 1: (a) Self-healing composite coupons made from Surlyn 8940 and carbon fiber; (b) proposed application of the self-healing layer.

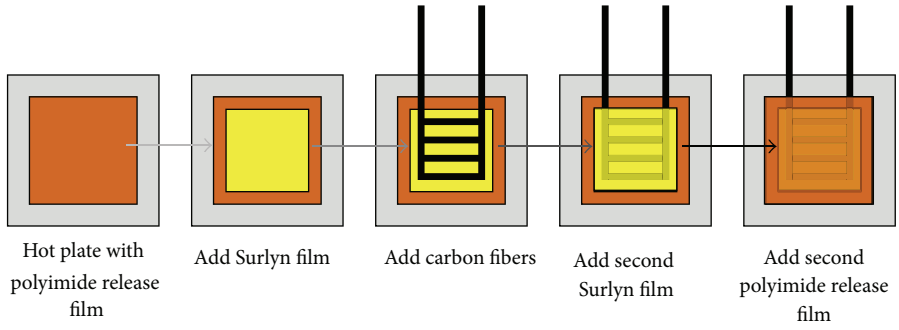

FIGURE 2: Fabrication of the self-healing composite.

221 m/s to the polymer. The virgin Surlyn coupons measuring 7.62 cm × 7.62 cm and 1.2 mm in thickness are used in the medium-velocity impact test setup. The air gun used in this experiment has a manual pumping mechanism to deliver the projectile, and the exit velocity of the projectile is rated at 221 m/s for 10 pumps. The air gun has a safety mechanism that prevents the pressure in the chamber from increasing beyond 10 pumps. In order to quantify the effect of velocity on healing in the sample, the number of pumps was also varied to observe the effect of the projectile velocity on healing in the sample. Impact experiments were carried out at 5 pumps, 7 pumps, 10 pumps, and 12 pumps to observe the effect of autonomous healing in the sample. In order to compare the effect of self-healing in Surlyn, teflon coupons of identical thickness were subject to impact experiments in this setup. From initial observations, it is noted that the projectile traveling at ≈145 m/s (corresponding to 7 pumps) does not penetrate the sample all the way through. From the experiments, it was observed that 3 out of 5 trials resulted in the projectile to remain lodged in Surlyn coupon as shown in Figure 3(c). If the pump on the air gun was primed for 10 pumps (≈221 m/s projectile velocity), it is observed that the projectile penetrates and exits the sample as shown in Figure 3(d). The resulting crater in the sample appears to have come together, and there is no continuous hole from one side of the membrane to the other as seen in the control teflon sample in Figure 3(e). It should be noted that the diameter of the projectile is ≈4.5 mm, and the resulting crater measures less than 1 mm. It is observed that fissures are formed in the crater walls that radiate towards the center of the crater following the path of the projectile. This initial qualitative assessment and the formation of fissures in the sample after the impact damage event serve as the motivation for subsequent resistive heating and healing of the sample.

2.3. Resistive Heating and Healing. It is anticipated that the samples from medium-velocity impact characterization experiments were subjected to subsequent resistive heating using carbon fibers in the application environment. In order to demonstrate the healing from resistive heating, the samples from impact experiments are subjected to resistive heating. Additionally samples are subjected to simulated damage, and healing of this simulated damage is demonstrated through resistive healing. A sample shown in Figure 4 is fabricated with threads evenly dispersed in Surlyn. Electrical resistance of the embedded carbon fiber in this sample is measured to be 6 Ω. A surface level damage is simulated in the sample using an x-acto knife without damaging the carbon fibers. Resistive heating of the sample for an applied electrical field is characterized through infrared (IR) bolometry. The IR images of resistive heating in the composite lead to better understanding of heat transfer and temperature distribution for healing a simulated damage. IR images are recorded using a Fluke Ti25 thermal imaging camera on a sample

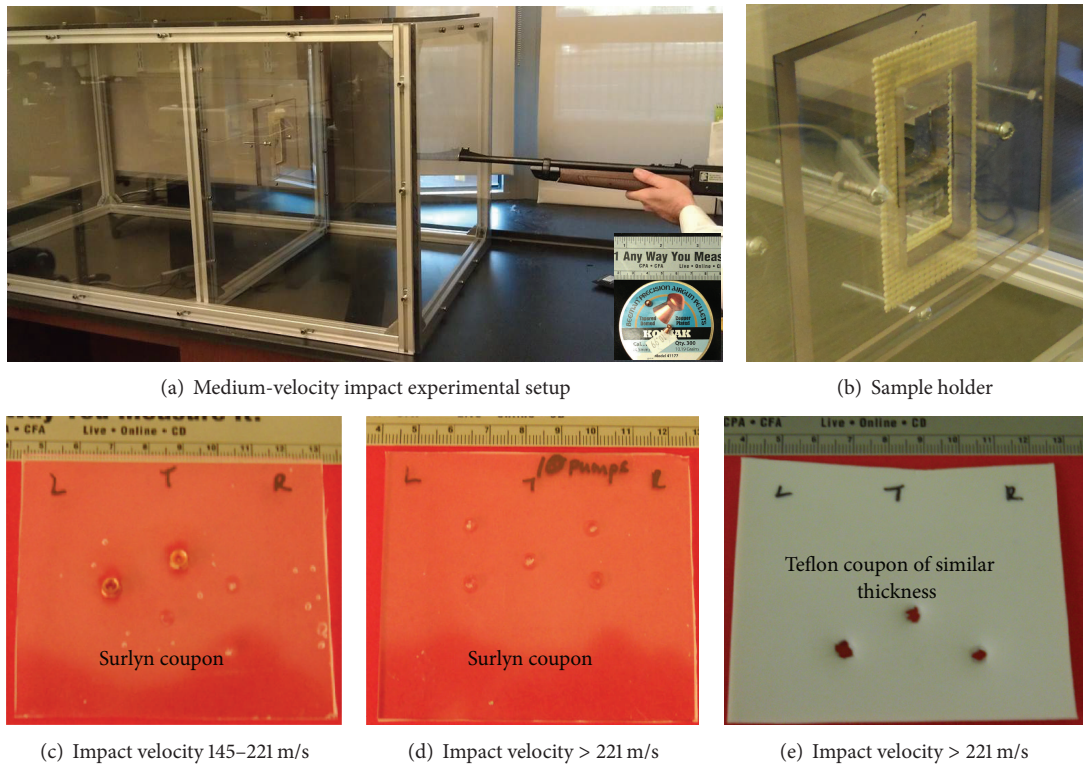

(a) Medium-velocity impact experimental setup

(b) Sample holder

(c) Impact velocity 145–221 m/s

(d) Impact velocity > 221 m/s

(e) Impact velocity > 221 m/s

Figure 3: Experimental setup for medium-velocity impact experiments, samples after impact.

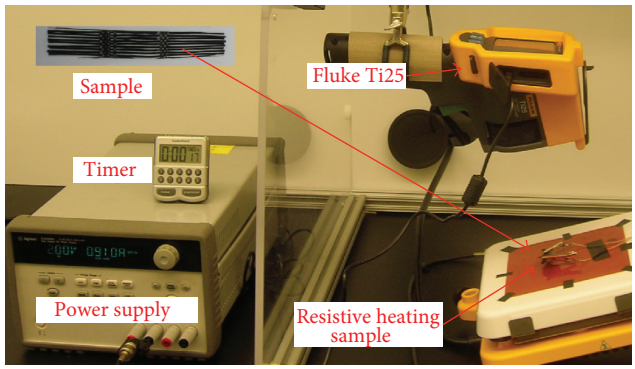

Figure 4: Resistive heating and healing demonstration in the self-healing composite. The power supply leads are connected to the sample. As the experiment begins, the timer is used so that thermal images can be acquired at certain time intervals.

shown in Figure 4. The electrical resistance of carbon fibers in the sample is measured using Autolab PGSTAT 128N FRA software to be 3.5 Ω. Heat generated in the carbon fiber layer and hence the changes in the temperature of the Surlyn layer in the composite are recorded for various applied voltages (2 V, 3 V, and 5 V) every 15 s for 1 min. The experimental setup for IR bolometry is shown in Figure 4. The electrical power applied to the sample to heal the material of the aforementioned voltages correspond to 1.2 W, 2.6 W, and 7.2 W.

The following important observations are derived from these experiments. Firstly, when a higher power is applied, more heat is generated in the sample and higher temperatures are achieved. Secondly, each experiment follows a definite trend of approaching a steady state temperature distribution. As heat generation due to Joule heating balances heat transfer out of the sample, the sample approaches a steady state temperature distribution. Finally, as the sample reaches the melt temperature, Surlyn melts around the damage and closes the damage. Based on these observations, it is inferred that there is a minimum power input required to elevate the temperature of the sample to reach melt temperature and heal any damage in the sample. Any higher power input will heat the sample to a higher temperature nonuniformly and heal the damage but not effectively.

Thus, healing is qualitatively demonstrated in this sample in Figure 5 by flexing the sample and observing the region near the damage before and after the application of electric field. It is also observed that the thickness of the sample does change during the healing process.

3. Healing Characterization

The qualitative observations made during medium-velocity experiments indicated a minimum velocity required for the projectile to pass through the sample and heal the sample, and resistive heating experiments indicated an optimal power required to uniformly heat the site of damage for complete healing. The following characterization experiments are designed to quantify healing of a damage as a function of power input (voltage and sample resistance) and time. This is followed by a finite-element model to optimize the

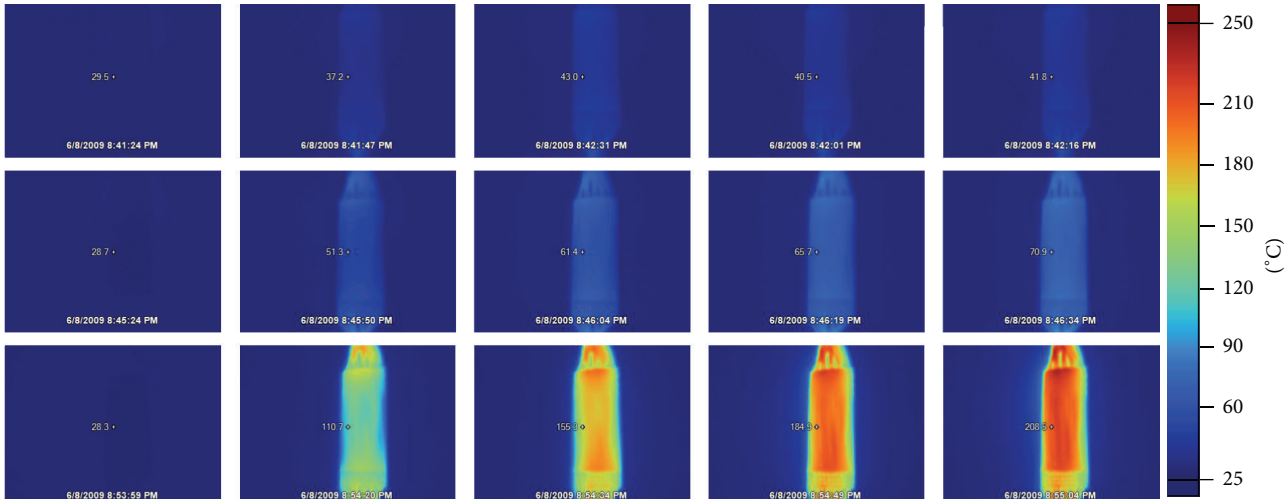

Figure 5: Thermal image results of resistive heating experiment. The sample is heated at 1.2 W (row 1), 2.6 W (row 2), and 7.2 W (row 3). Test duration increases from $t = 0$ at left to $t = 60$ s at right, in 15 s intervals.

distribution of carbon fiber bundles in the composite for uniform heating and healing.

3.1. Self-Healing from Medium-Velocity Impact. The initial observations led to conclusively establishing the following aspects of self-healing from medium-velocity impact experiments.

(i) A minimum velocity is required for the projectile to penetrate the sample.

(ii) The unique geometry of the projectile will leave fissures in the surface and through the thickness of the polymer, without a see-through hole in the sample.

(iii) The fissures can be represented as surface cracks in the sample that can be subsequently healed from resistive heating of the sample.

In order to quantify the residual damage in the sample from medium-velocity impact, the samples from these experiments were sputtered with gold or platinum and imaged under scanning electron microscope. From these images, it is observed that the effective size of the damage at the center of the crater is on the order of 200 μm, the fissures in the crater measure on the order of 500–800 μm, and the depth of the damage along the crater walls is on the order of 25–100 μm. The formation of the fissures and the feature size on the crater walls are anticipated to be dependent on the angle of impact, projectile material, velocity of impact, stiffness of the polymer, and so forth. This study was restricted to demonstrate the ability to completely heal one such damage through a combination of autonomous healing response and resistive heating. The samples subjected to medium-velocity impact were subjected to a simulated resistive heating on a hot plate for an equivalent duration at a temperature of 100°C. The micrographs in Figure 6 show the effect of the impact on the samples and the subsequent healing of the damage observed in the sample from heating. The features observed in Figures 6(a) and 6(b) were taken as templates for creating simulated damage in characterization of healing through resistive heating. In subsequent characterization, this work establishes the power requirements and time duration required to completely remove a similar damage from Surlyn.

3.2. Width-Heal Ratio (WHR). The self-healing material intended for use as thin membranes without a particular need for supporting structural load requires a new metric to quantify healing. The contemporary methods used for characterizing self-healing presented in the detailed review of self-healing materials by Blaiszik et al. [32] are not applicable for thin membranes and especially electrical wire-insulation materials. The presence of surface cracks and damages in a typical aircraft wire-insulation layer will result in arc tracking across the edges of a damage and potentially lead to catastrophic damage from electrical fire [33]. It is necessary that the healing technique for the intended application removes the surface crack, and the characterization metric quantifies the width of the damage before and after healing.

In order to accurately quantify healing, a jig consisting of a linear slide with a razor blade is devised to create a controlled damage in a repeatable manner. A fixed mass mounted on top of the slide applies a constant force to the razor blade as it is dragged across the sample. The depth of the damage in the sample is varied by adding different weights to the linear slide. The jig with a schematic of the damage in the sample is shown in Figure 7. The fixed mass is selected such that the triangular section of the blade is not completely buried in the sample as shown in the inset in Figure 7. This ensures that the damage width is proportional to the depth of the cut in the sample and is easily measurable under a Carl-Zeiss Axiovert 35 microscope at 100x or 400x.

The width of the damage is measured at five locations along the damage and averaged to report the average width before healing (w_b). The sample is heated by the application of an electrical field at the ends of the carbon fiber for a finite

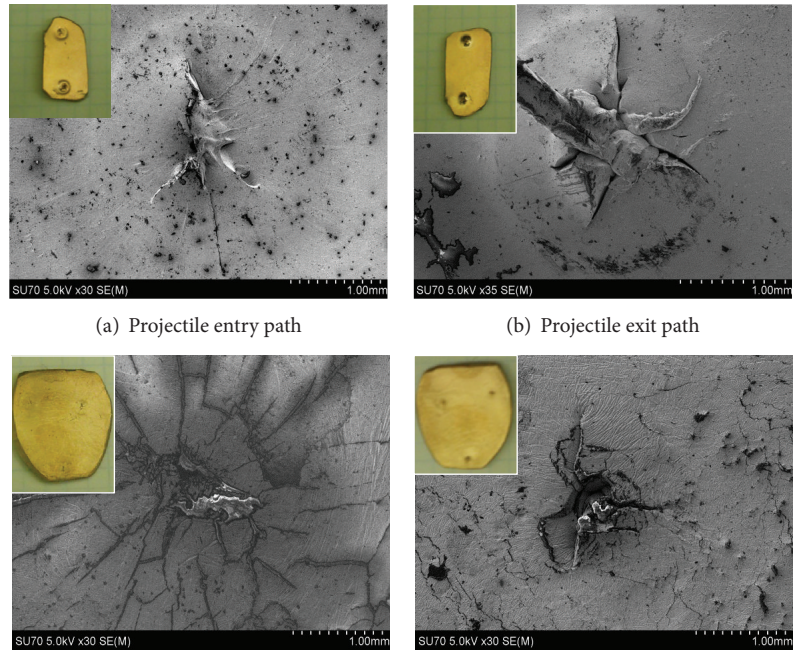

(a) Projectile entry path (b) Projectile exit path

(c) Projectile entry path (d) Projectile exit path

FIGURE 6: SEM images of Surlyn samples after impact and subsequent healing: (a) entry path damage, (b) exit path damage, (c) entry path damage, then subsequently healed, and (d) exit path damage, then subsequently healed.

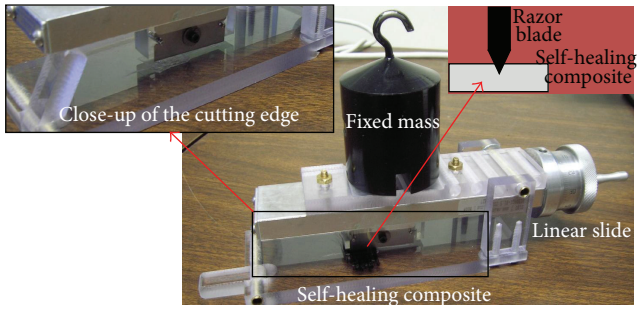

FIGURE 7: Jig for producing a controlled and repeatable damage for healing characterization experiments. Insets show a close-up of the blade with a sample, and the schematic shows the geometry of razor blade used to damage Surlyn.

duration as determined by the experiment, allowed to cool, and the crack width is measured. This measured width of the damage is reported as the value after healing (w_a).

The damage width before and after healing is used to calculate the width-heal ratio (WHR) as shown in (1). This metric is typically reported in this paper as a percentage and is found to be useful in estimating the effectiveness of the healing process. The width-heal ratio (WHR), given by

$$\text{WHR} = \frac{w_b - w_a}{w_b}, \tag{1}$$

is determined for different input conditions for healing a damage. Owning to the nature of this self-healing metric, it is limited in its application to materials with thin cross-sections. In this paper, we have restricted our application to coupons less than 500 μm in thickness.

Two batches of composite samples measuring 10 mm × 20 mm and differing in the arrangement of carbon fibers are prepared for quantitative resistive heating/healing tests. The first batch has carbon fibers evenly dispersed in the sample and measure 0.75 mm in thickness. In the second batch, carbon fibers are woven into the composite as 12 discrete 1 k bundles. In both batches, the samples contain carbon fibers that are 5% by mass with 1.8 Ω of electrical resistance. A controlled damage is introduced on the samples by placing 200 g and 1000 g masses on the jig (Figure 7). The average width of the damage in the sample for the two masses is found to be 14.4 μm and 28.3 μm and sufficiently spaced apart for healing characterization. The following tests are performed for healing characterization.

(i) Varying energy input.

(ii) Varying power input.

Varying Energy Input. The objective of the first test is to vary the duration for which a constant power is applied to the sample and thus vary the energy input. An electrical potential of 1 V is applied to the sample for durations of 2 min, 5 min, and 10 min. Electrical energy inputs to the sample at a constant power of 0.62 W corresponding to the different durations are 75 J, 185 J, and 370 J. The damage width is measured under a 400x optical microscope after the sample cools down, and WHR is calculated.

It is observed from Figure 8 that WHR is less than 10% after 2 minutes. As the potential is applied to the sample for a longer duration, the WHR increases to 50–60%. The

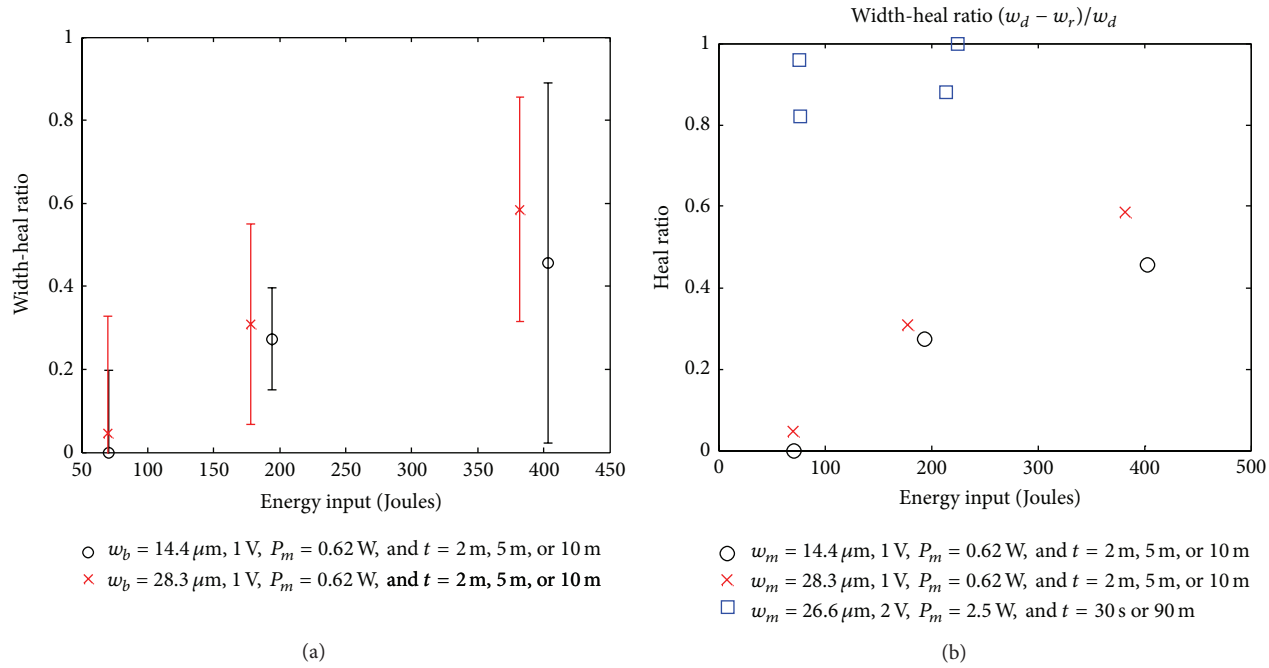

FIGURE 8: (a) Healing results show that WHR increases as energy input increases. Increasing crack width has a smaller effect on WHR. (b) Healing results show that WHR increases at higher electrical power input.

mean WHR and bounds from experiments reported in Figure 8(a) are student-t distribution from five samples. The large variation in the results is attributed to the variations in the distribution of carbon fibers in the sample resulting from manual fabrication methods. From this experiment, it is established that WHR increases with the amount of electrical energy applied to the sample. It should also be noted that WHR and healing in the sample are not affected by the damage width. Thus, *for a given power input or rate of heating, WHR increases with the duration and reaches a steady state.*

Varying Power Input. The trials in this experiment are performed to characterize the power required to heal a damage. Another set of samples with similar electrical and physical properties ($R_{\text{mean}} = 1.7\,\Omega$, $w_d = 26.6\,\mu$m, and $t = 0.75$ mm) is prepared, and the duration of the experiment and power are selected so that the energy input to the composite will be comparable with the previous experiment. The input power to the carbon fiber is increased to 2 V, and durations of 30 s and 90 s are chosen. These parameters correspond to 75 J and 185 J of electrical energy applied to the sample. It is observed that the WHR from these experiments are above 80%, and in some samples, the damage disappears from the surface. The data in Figure 8 shows that a high WHR is achieved in a shorter duration by increasing the power and within a given energy envelope. This result is significant for aerospace applications where healing the material is limited by available energy. Thus, *for a given energy envelope, effectiveness of the healing process is dependent on the power input or rate of heating.*

Similar trends are observed from experiments performed on composite samples with discrete set of carbon fiber bundles. It should be noted that Surlyn has low conductivity, and the distribution of fibers is observed to have an effect on uniform heating and healing in the sample. The IR image in Figure 9(b) of the heated sample shows the temperature distribution in the sample. Based on the observations in these experiments, the following conclusions can be drawn.

(i) Healing is more dependent on the rate of heating (input power) than energy (duration). In tests with input energy of about 75 J almost no healing is observed at 0.62 W, and 80% healing is observed at 2.5 W. Similarly, for an energy envelop of 200 J, 30% healing is observed at 0.62 W, and 80% healing is observed at 2.5 W.

(ii) With a proper distribution of carbon fibers in Surlyn and at a sufficient power input, it is possible to completely heal a damage.

Minimum Time for Healing. The observations from the previous experiments indicate that there is a minimum time required for maximum healing. Thus any energy input into the composite to heal a damage will be ineffective. The following experiment is performed to find the minimum time required to heal a damage in the composite. For the following experiments, discrete bundles of carbon fibers embedded as a network of parallel resistors inside Surlyn and shown in Figure 9(b) are used. In addition, this experiment will also be used to investigate the time required to heal different damage widths in the sample. The samples are heated at a constant rate (constant power input) in these experiments. Due to the complexity in sample geometry, a wide variation in electrical resistance of the carbon fiber layer is observed and shown in Figure 10(a). The samples have six discrete carbon fiber

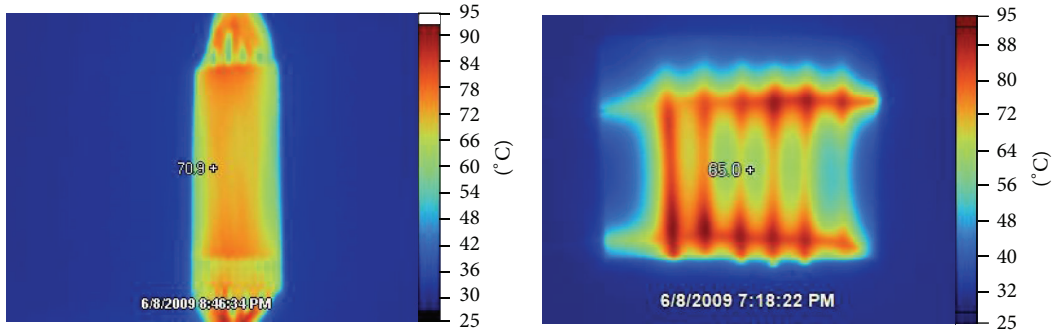

(a) (b)

Figure 9: Distribution of carbon fiber heating elements affects temperature distribution in the composite. Uniform fiber distribution (a) and parallel network arrangement (b).

bundles, measure 0.72 mm thick, and have a mean resistance of 8 Ω. Controlled damages of widths of 61.8 μm, 69.6 μm, and 96.4 μm are introduced in the samples using 200 g, 300 g, and 500 g masses in the jig. Due to higher resistance of the carbon fiber layer, a higher electrical potential is applied to the samples to apply the same power and energy input from the previous experiments. Healing tests were conducted by applying a constant 4 V to the sample for 15 s, 30 s, 45 s, or 60 s. Due to variation in sample resistance, current through the sample, power consumed, and heat generated varied considerably. The results from trials in this experiment are shown in Figure 10(b). Despite the variations between samples, the trends similar to the previous experiment are observed from the results. As healing duration increases, WHR increases, as expected. When heated for a sufficient duration, the areas around the damage reache the melt temperature of Surly and heal the damage. In most samples with small damages, the damage disappeared completely. The location of a damage with respect to the carbon fiber bundle in the sample played an important role in healing. This is due to the fact that the temperature distribution in the sample is highly influenced by the thermal properties of Surlyn. All the aforementioned experiments established that the Surlyn surface with damage should reach the melt temperature for effective healing. In order to predict the healing characteristics of the composite accommodating the subjectiveness of the sample geometry and the possible wide-ranging applications, the temperature results from these experiments are used to predict the temperature profile in the sample.

3.3. Modeling Resistive Heating in the Composite. The experiments demonstrate that the damaged area should reach the melt temperature of Surlyn for the damage to heal completely. The existing models [13, 19, 34–36] for predicting the healing characteristics of self-healing materials do not exactly capture the temperature distribution of this thermoplastic ionomer in the presence of carbon fibers. In order to predict healing in samples with different physical arrangements of Surlyn and carbon fiber in the composite, a multiphysics model is developed. This model takes different physical processes into account to predict the temperature near the damage site for an applied electrical potential to the carbon fibers. While this model does not account for all the physical conditions to fully design a resistive heating-based self-healing material, it presents a framework that can be tailored to match various design configurations.

3.3.1. Governing Equations. The electrical current flowing through the carbon fibers generates heat from Joule heating and conducts heat to the surrounding Surlyn matrix. Resistive heating (Joule heating) is governed by Joules Law, and the thermal energy for an applied current I through the heating element is given by the formula

$$Q = Pt = I^2 Rt, \tag{2}$$

where Q is the amount of thermal energy, P is the power, t is time, and R is electrical resistance. Heat transfer by conduction in carbon fiber and Surlyn is governed by the general three-dimensional heat conduction equation

$$\frac{\partial^2 T}{\partial x^2} + \frac{\partial^2 T}{\partial y^2} + \frac{\partial^2 T}{\partial z^2} + \frac{\dot{q}}{k} = \frac{\rho c_p}{k}\frac{\partial T}{\partial t}, \tag{3}$$

where T is temperature, $\dot{q}$ is the heat flux, k is the thermal conductivity, ρ is the mass density, c_p is the specific heat capacity at constant pressure, and t is time. A prescribed temperature and convection condition are applied at the composite-air interface. The prescribed temperature condition, given by (4), is used to specify the initial temperature (21°C) of the entire model before the electrical field is applied. The convection boundary condition, given by (5), is used to model heat transfer out of the composite sample due to natural convection:

$$T_1 = T(x, y, z, t), \tag{4}$$

$$\left(k\frac{\partial T}{\partial x} + h_1 T\right)_{x=0} = h_1 T, \tag{5}$$

where h is the convection heat transfer coefficient.

3.3.2. Modeling Techniques. The model is developed and validated for samples with uniformly distributed carbon fiber

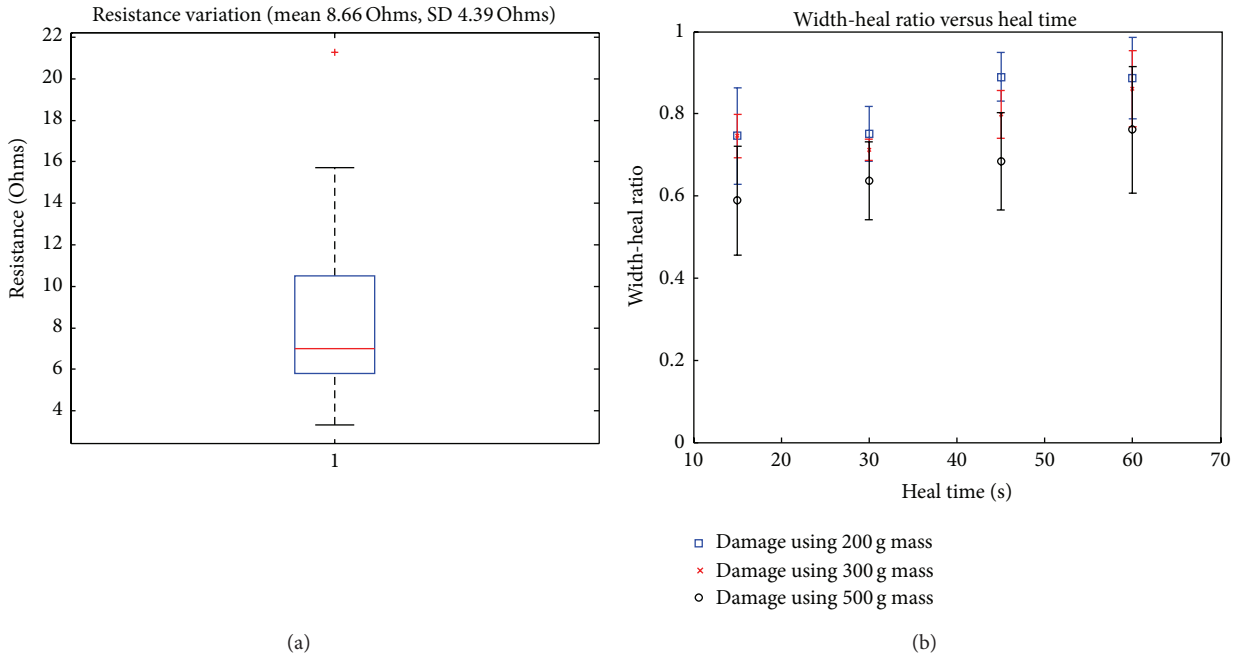

FIGURE 10: (a) Distribution of sample resistances. Mean is 8.66 Ω; standard deviation is 4.39 Ω. (b) Results of healing tests with network of parallel resistors samples. Results are shown for different simulated damage created on the coupons using weights in our fixture.

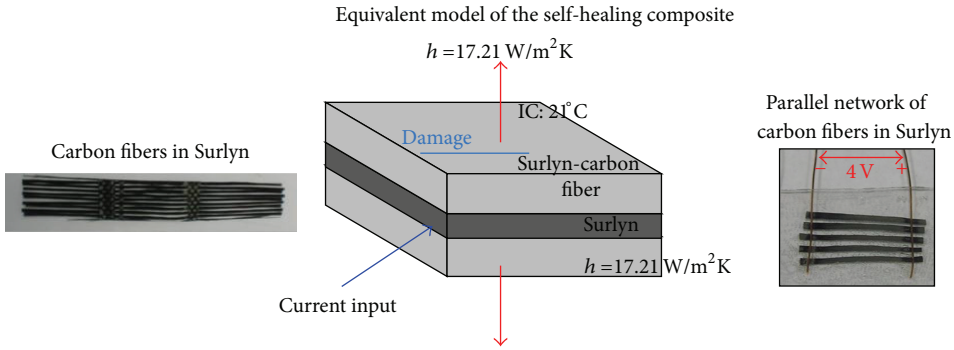

FIGURE 11: Configuration of the Surlyn/carbon fiber resistive heating sample modeled using finite-element method with boundary conditions. Model developed is validated for the sample on the left and used for predicting the temperature distribution with discrete bundles of carbon fibers.

threads as shown in the sample on the left in Figure 11. In these samples, the carbon fiber heating element is considered to be a continuous thin sheet, instead of individual threads. The resolution of the thermal imaging camera is larger than the distance between the threads, and hence the camera cannot distinguish between adjacent fiber bundles. This does not void the measurement but does not provide the spatial resolution to validate the results from the model.

The thickness of the carbon fiber layer is measured to be 0.05 mm and that of the Surlyn matrix enclosing the carbon fiber layer is 10 mm × 20 mm × 0.75 mm. The length of the carbon fiber heating elements is chosen to be 20 mm. Carbon fiber bundles are discretized using linear three-dimensional coupled thermal-electrical elements having eight nodes per element. Surlyn is discretized using linear three-dimensional heat transfer elements also having eight nodes per element. The carbon fiber layer is meshed with two elements through its thickness, eight elements across its width, and twenty elements along its length. Surlyn is meshed with four elements through its thickness, eight elements across its width, and twenty elements along its length.

Two analysis steps are created. The first step is a steady state heat transfer step and is used for bringing the entire model up to room temperature of 21°C. A specified temperature boundary condition of 21°C is applied to the sample, and the analysis is run to steady state conditions. The second step, a transient coupled thermal-electrical analysis step, is created to model Joule heating and subsequent heat transfer. In order to facilitate comparisons with resistive heating experiment, transient Joule heating analysis is run for a duration of 60 s. Electrical current is applied to the end nodes of the carbon fiber. In order to apply an accurate value of current flowing

Table 1: Properties of air.

β	ν	α	k
$0.0033\,K^{-1}$	$16.2 \times 10^{-6}\,m^2/s$	$22.9 \times 10^{-6}\,m^2/s$	0.0265 W/mK

Table 2: Heat transfer coefficient for model simulations of different resistive heating experiments.

Experiment	Ra_L	Nu_L	h (W/m^{2}K)
2 V	13962	5.87	7.78
3 V	34905	7.38	9.78
5 V	131244	10.28	13.62

through the sample in the model, the resistance of the carbon fiber is measured using an Autolab PGSTAT 12 analyzer running FRA software and is found to be 3.3 Ω. Resistive heating experiments conducted on this sample at 2 V, 3 V, and 5 V resulted in current draws of 0.571 A, 0.857 A, and 1.429 A, respectively. In the model it is assumed that all electrical energy is converted to thermal energy by setting the Joule heat fraction to be equal to one. Heat is transferred from the carbon fiber heating element to the surrounding Surlyn because the two materials are in thermal contact with one another. In this model thermal contact is assumed to be ideal, and there is no resistance to heat flow at the interface of the two materials.

The first step in estimating the convective heat transfer coefficient is to calculate the Rayleigh number using the following equation:

$$\mathrm{Ra}_L = \frac{g\beta\left(T_s - T_\infty\right)L^3}{\nu\alpha}, \tag{6}$$

where g is acceleration due to gravity, β is the thermal expansion coefficient, T_s is the surface temperature, T_∞ is the far field temperature, ν is the kinematic viscosity, α is the thermal diffusivity, and L is the length. Thermal images of resistive heating experiments on the same sample geometry, shown in Figure 5, are used to determine surface temperatures. The convection heat transfer coefficients which are calculated for each case to accommodate different temperature profiles are observed in the experiments. Surface temperature values of 41°C, 71°C, and 209°C after 60 s correspond to 2 V, 3 V, and 5 V applied to the sample, respectively. The thermal properties of air at room temperature used in the model are listed in Table 1. The Nusselt numbers are calculated using Rayleigh numbers in $\mathrm{Nu}_L = 0.54 \cdot \mathrm{Ra}_L^{1/4}$, and the convective heat transfer coefficients are calculated using the Nusselt numbers in $h = (k/L) \cdot \mathrm{Nu}_L$, where k is the thermal conductivity of the air, L is characteristic length, and h is the convective heat transfer coefficient. The data in Table 2 lists the results of the Rayleigh numbers, Nusselt numbers, and heat transfer coefficients.

The convective heat transfer boundary condition is applied to the outer surfaces of Surlyn as shown in Figure 11. Convective heat transfer out of the sides of the carbon fiber and the end of the sample is ignored due to the small area. Material properties for Surlyn and carbon fiber are listed in Table 3. In addition, variations in electrical conductivity with temperature is accounted by including the temperature coefficient of resistivity of carbon. The values of the conductivity of carbon fiber ($\alpha = -0.0005$) at elevated temperatures are estimated using linear interpolation using $R = R_o[1 + \alpha(T - T_o)]$. Material properties for carbon fiber are constant throughout the volume of carbon fiber; properties of Surlyn are assumed constant throughout the volume of Surlyn.

Table 3: Material properties of Surlyn and carbon fiber (CF).

$\rho_{\mathrm{Surlyn}} =$	950	kg/m^3
$k_{\mathrm{Surlyn}} =$	0.246	W/mK
$c_{p\mathrm{Surlyn}} =$	2100	J/kgK
$\rho_{\mathrm{CF}} =$	1800	kg/m^3
$k_{\mathrm{CF}} =$	15	W/mK
$c_{p\mathrm{CF}} =$	1000	J/kgK
$\sigma_{\mathrm{CF},T=21^\circ\mathrm{C}} =$	68965.5	1/Ωm

3.3.3. Modeling Results. The objective of this finite-element model is to develop a framework for predicting the temperature distribution on the surface of the sample with time for various rates of heating. In order to evaluate the accuracy of the model, simulation results are compared to temperature measurements from resistive heating experiments made using an infrared (IR) camera. Measurements on resistive heating samples were made on samples with an even distribution of carbon fibers, as shown in Figure 11, and compared to temperature profiles on the sample from IR imaging as shown in Figure 5. Samples were healed at equivalent power levels to resistive heating/healing experiments described in the previous section. Temperature data as a function of time was extracted from the finite-element model for the center node on the outer surface of Surlyn and shown in Figure 12, representing the average surface temperature of Surlyn.

Finite-element results predict higher surface temperature and slower temperature rise than thermal images of resistive heating experiments indicate. There are several potential sources of error leading to inaccuracies in the model. First, the electrical conductivity of carbon fiber layer used in the resistive heating experiments and interface losses are difficult to estimate accurately. Second, we believe that not all of the electrical current is converted to heat in the carbon fibers. Last but not least, the convective heat transfer rate between Surly and air is not a constant and dependent on the surface temperature of Surlyn. This FEM provides the ability to predict the temperature distribution in the polymer from resistive heating for subsequent design.

4. Conclusions

The results reported in this paper demonstrate the ability of the polymer matrix to come together and close the path of penetration of a medium-velocity projectile (≈229 m/s). Subsequent heating of polymer using embedded carbon fiber means demonstrates the ability of the polymer to further heal

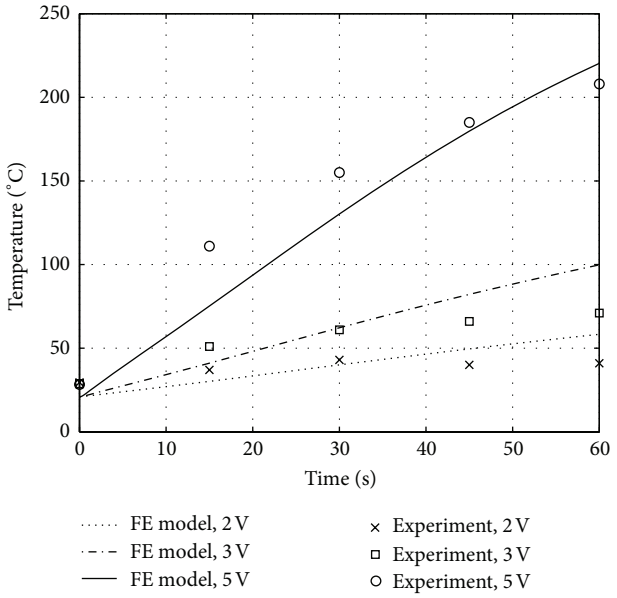

Figure 12: Model data compared to temperature measurements made on resistive heating experiments using the thermal imaging camera.

and close any damage from this impact. The polymer matrix made out of Surlyn melts at 95°C from the heat generated in the carbon fiber layer and heals any surface and through-thickness damage in the polymer matrix. The carbon fiber layer has low resistance and hence requires 2-3 W of electrical power in a 20 mm × 10 mm panel to heal any damage in the polymer. The mathematical model developed in this work characterizes the heating characteristics of Surlyn-carbon fiber composites for two configurations of carbon fiber in the polymer. Once the composite is heated and held near the glass transition temperature of the polymer matrix, our experiments show that a surface damage in the polymer can be healed completely. A new metric, referred to as width-heal ratio that characterizes the melt flow around the damage, has been developed to represent healing in the polymer. The experiments demonstrate the damage in the material can be completely healed (with a width-heal ratio (WHR) > 0.9) by heating the damaged area to the melt temperature in less than 30 s. Thus, the work presented in this paper demonstrates a self-healing composite material made from Surlyn and carbon fibers that can be used as the self-healing layer for various aerospace applications.

Conflict of Interests

The authors declare no possible conflict of interests.

Acknowledgments

The authors would like to acknowledge the financial support from NASA through WIISP Program (STTR Contract no. NNK06MB01C) and SHIELD Program (STTR Contract no. NNX11CI22P). The authors would also like to acknowledge support from Dr. Timothy Long, Department of Chemistry, Virginia Tech, for allowing them to use his lab facilities for sample fabrication and technical assistance during the performance of this work. The authors would like to acknowledge Capt. Grant Warren's (VCU Police) assistance in carrying out the experiments in Sundaresan's lab in Virginia Commonwealth University.

References

[1] E. N. Brown, N. R. Sottos, and S. R. White, "Fracture testing of a self-healing polymer composite," *Experimental Mechanics*, vol. 42, no. 4, pp. 372–379, 2002.

[2] J. D. Rule, N. R. Sottos, and S. R. White, "Effect of microcapsule size on the performance of self-healing polymers," *Polymer*, vol. 48, no. 12, pp. 3520–3529, 2007.

[3] B. J. Blaiszik, N. R. Sottos, and S. R. White, "Nanocapsules for self-healing materials," *Composites Science and Technology*, vol. 68, no. 3-4, pp. 978–986, 2008.

[4] H. Andersson, M. Keller, J. Moore, N. Sottos, and S. White, *Self Healing Polymers and Composites, Vol. 100 of Springer Series in Materials Science*, Springer, Amsterdam, The Netherlands, 2008.

[5] R. S. Trask, H. R. Williams, and I. P. Bond, "Self-healing polymer composites: mimicking nature to enhance performance," *Bioinspiration and Biomimetics*, vol. 2, no. 1, pp. P1–P9, 2007.

[6] H. R. Williams, R. S. Trask, A. C. Knights, E. R. Williams, and I. P. Bond, "Biomimetic reliability strategies for self-healing vascular networks in engineering materials," *Journal of the Royal Society Interface*, vol. 5, no. 24, pp. 735–747, 2008.

[7] H. R. Williams, R. S. Trask, P. M. Weaver, and I. P. Bond, "Minimum mass vascular networks in multifunctional materials," *Journal of the Royal Society Interface*, vol. 5, no. 18, pp. 55–65, 2008.

[8] K. S. Toohey, N. R. Sottos, J. A. Lewis, J. S. Moore, and S. R. White, "Self-healing materials with microvascular networks," *Nature Materials*, vol. 6, no. 8, pp. 581–585, 2007.

[9] H. R. Williams, R. S. Trask, and I. P. Bond, "Self-healing composite sandwich structures," *Smart Materials and Structures*, vol. 16, no. 4, pp. 1198–1207, 2007.

[10] A. M. Aragón, J. K. Wayer, P. H. Geubelle, D. E. Goldberg, and S. R. White, "Design of microvascular flow networks using multi-objective genetic algorithms," *Computer Methods in Applied Mechanics and Engineering*, vol. 197, no. 49-50, pp. 4399–4410, 2008.

[11] C. J. Norris, J. A. P. White, G. McCombe, P. Chatterjee, I. P. Bond, and R. S. Trask, "Autonomous stimulus triggered self-healing in smart structural composites," *Smart Materials and Structures*, vol. 21, no. 9, Article ID 094027, 2012.

[12] T. Yang, C. Wang, J. Zhang, S. He, A. Mouritz, and "Toughening and self-healing of epoxy ma- trix laminates using mendable polymer stitching," *Composites Science and Technology*, vol. 72, no. 12, pp. 1396–1401, 2012.

[13] V. Privman, A. Dementsov, and I. Sokolov, "Modeling of self-healing polymer composites reinforced with nanoporous glass fibers," *Journal of Computational and Theoretical Nanoscience*, vol. 4, no. 1, pp. 190–193, 2007.

[14] R. S. Trask, G. J. Williams, and I. P. Bond, "Bioinspired self-healing of advanced composite structures using hollow glass fibres," *Journal of the Royal Society Interface*, vol. 4, no. 13, pp. 363–371, 2007.

[15] A. Kousourakis and A. P. Mouritz, "The effect of self-healing hollow bres on the mechanical properties of polymer composites," *Smart Materials and Structures*, vol. 19, no. 8, Article ID 085021, 2010.

[16] T. Yin, M. Z. Rong, J. Wu, H. Chen, and M. Q. Zhang, "Healing of impact damage in woven glass fabric reinforced epoxy composites," *Composites A*, vol. 39, no. 9, pp. 1479–1487, 2008.

[17] J. L. Moll, S. R. White, and N. R. Sottos, "A self-sealing fiber-reinforced composite," *Journal of Composite Materials*, vol. 44, no. 22, pp. 2573–2585, 2010.

[18] X. Chen, F. Wudl, A. K. Mal, H. Shen, and S. R. Nutt, "New thermally remendable highly cross-linked polymeric materials," *Macromolecules*, vol. 36, no. 6, pp. 1802–1807, 2003.

[19] N. Kwok and H. T. Hahn, "Resistance heating for self-healing composites," *Journal of Composite Materials*, vol. 41, no. 13, pp. 1635–1654, 2007.

[20] J. S. Park, K. Takahashi, Z. Guo et al., "Towards development of a self-healing composite using a mendable polymer and resistive heating," *Journal of Composite Materials*, vol. 42, no. 26, pp. 2869–2881, 2008.

[21] Kalista, *Self-Healing of thermoplastic poly(Ethylene-Co-Meth-acrylic Acid) copolymers following projectile puncture [Ph.D. thesis]*, Virginia Polytechnic Institute and State University, Burruss Hall, Va, USA, 2003.

[22] S. J. Kalista and T. C. Ward, "Thermal characteristics of the self-healing response in poly(ethylene-co-methacrylic acid) copolymers," *Journal of the Royal Society Interface*, vol. 4, no. 13, pp. 405–411, 2007.

[23] R. J. Varley and S. Van der Zwaag, "Development of a quasi-static test method to investigate the origin of self-healing in ionomers under ballistic conditions," *Polymer Testing*, vol. 27, no. 1, pp. 11–19, 2008.

[24] R. J. Varley and S. van der Zwaag, "Autonomous damage initiated healing in a thermo-responsive ionomer," *Polymer International*, vol. 59, no. 8, pp. 1031–1038, 2010.

[25] K. Pingkarawat, C. Wang, R. Varley, and A. Mouritz, "Effect of mendable polymer stitch density on the toughening and healing of delamination cracks in carbon-epoxy laminates," *Composites A*, vol. 50, pp. 20–30, 2013.

[26] C. C. Owen, *Magnetic induction for in-situ healing of polymeric material [M.S. thesis]*, Virginia Polytechnic Institute and State University, Burruss Hall, Va, USA, 2006.

[27] D. Y. Wu, S. Meure, and D. Solomon, "Self-healing polymeric materials: a review of recent developments," *Progress in Polymer Science*, vol. 33, no. 5, pp. 479–522, 2008.

[28] J. A. Carlson, J. M. English, and D. J. Coe, "A flexible, self-healing sensor skin," *Smart Materials and Structures*, vol. 15, no. 5, pp. N129–N135, 2006.

[29] A. J. Patel, N. R. Sottos, E. D. Wetzel, and S. R. White, "Autonomic healing of low-velocity impact damage in fiber-reinforced composites," *Composites A*, vol. 41, no. 3, pp. 360–368, 2010.

[30] T. Swait, A. Rauf, R. Grainger et al., "Smart composite materials for self-sensing and self-healing," *Plastics, Rubber and Composites*, vol. 41, no. 4-5, pp. 215–224, 2012.

[31] K. Hargou, K. Pingkarawat, A. Mouritz, and C. Wang, "Ultrasonic activation of mend- able polymer for self-healing carbonepoxy laminates," *Composites B*, vol. 45, no. 1, pp. 1031–1039, 2013.

[32] B. J. Blaiszik, S. L. B. Kramer, S. C. Olugebefola, J. S. Moore, N. R. Sottos, and S. R. White, "Self-healing polymers and composites," *Annual Review of Materials Research*, vol. 40, pp. 179–211, 2010.

[33] M. Stavnes and A. Hammoud, "Assessment of safety in space power wiring systems," *IEEE Aerospace and Electronic Systems Magazine*, vol. 9, no. 1, pp. 21–27, 1994.

[34] A. C. Balazs, "Modeling self-healing materials," *Materials Today*, vol. 10, no. 9, pp. 18–23, 2007.

[35] A. Dementsov and V. Privman, "Percolation modeling of conductance of self-healing composites," *Physica A*, vol. 385, no. 2, pp. 543–550, 2007.

[36] S. Maiti, C. Shankar, P. H. Geubelle, and J. Kieffer, "Continuum and molecular-level modeling of fatigue crack retardation in self-healing polymers," *Journal of Engineering Materials and Technology*, vol. 128, no. 4, pp. 595–602, 2006.